A large π-conjugated ligand in metal-organic framework as opticalswitch to regulate the electron transfer pathway for highly selective reduction of CO2 to CH4

Pei-Qin Liao (liaopq3@mail.sysu.edu.cn)
Sun Yat-sen University https://orcid.org/0000-0001-5888-1283
Yuanyuan Liu
Nanjing University
Hao-Lin Zhu
Sun Yat-sen University
Ning-Yu Huang
Sun Yat-sen University
Xiao-Ming Chen
Sun Yat-sen University https://orcid.org/0000-0002-3353-7918

Article

Keywords: Visible Light, Photocatalytic Reduction, in-situ Infrared Spectroscopy, Mott-Schottky Measurements, Lowest Unoccupied Molecular Orbital, Photoswitch

Posted Date: March 26th, 2021

DOI: https://doi.org/10.21203/rs.3.rs-334383/v1

Abstract

Here, we report a Cu-based metal-organic framework (Cu-DBC), constructed by the large π-conjugated ligand dibenzo-[g,p]chrysene-2,3,6,7,10,11,14,15-octaol and the square-pyramidal CuO5 nodes, as the photo-coupled electrocatalysts for CO2 reduction to CH4. Under visible light, it exhibits high performance for photocatalytic reduction of CO2 to CH4 with selectivity of 100% and rate of 1.04 μmol g-1 h-1, without additional photosensitizer. Importantly, at -1.4 V vs. RHE, it exhibits high performance for photo-coupled electroreduction of CO2 to CH4 with a Faradaic efficiency (CH4) of 93% and current density of 10.4 A g-1. Theoretical calculations, in-situ infrared spectroscopy investigation and Mott–Schottky measurements showed that the large conjugated ligand in Cu-DBC has the suitable lowest unoccupied molecular orbital (LUMO) to match well with the reduction potential of CO2/CH4 and serves as a photoswitch to regulate electron transfer pathway to the metal center, resulting highly selective photocatalytic reduction or photo-coupled electroreduction of CO2 to CH4.

Introduction

The increase of atmospheric CO_2 has a severe impact on global climate and ecological environment.[1-6] Scientists have carried out extensive researches on catalytic transformations of CO_2 molecules into high value-added chemicals, such as methane[7-8] and ethylene.[9] However, the CO_2 reduction to hydrocarbons usually involves multi-electron transfer processes (*e.g.* 8 electrons for CH_4 and 12 electrons for C_2H_4), leading to slow kinetics and high overpotential.[10] Compared with traditional methods, such as thermal catalysis,[11] photocatalysis[12-13] and electrocatalysis,[14-15] the photo-coupled electrocatalytic CO_2 reduction (PECR) is a competitive method.[16-18] It has been suggested that light can induce the band bending,[19] thus reducing overpotential for CO_2 reduction and changing the catalytic pathways. In addition, the electrons and holes can be directionally separated in the external field, facilitating charge separation.[20] However, the studies in this field are very limited and challenging. Therefore, the development of new photo-coupled electrocatalyst system for CO_2 reduction is urgently necessary.

CO_2 reduction can generate a variety of products such as HCOOH, CO, CH_4 and C_2H_4, *etc*. To date, most of reported PECR catalysts were shown to convert CO_2 to CO or HCOOH, rather than high-value-added chemicals (*e.g.*, CH_4 and C_2 products).[17, 21-23] From the point of thermodynamics, it is possible to achieve high selectivity of CH_4 by rationally designing an electrocatalyst with the appropriate lowest unoccupied molecular orbital (LUMO) matching with the reduction potential of CO_2/CH_4 (-0.24 V) (Scheme 1). Among all the metal catalysts, Cu has been demonstrated to be capable of converting CO_2 into CH_4 and C_2 species, which is related to the appropriate interaction of *CO intermediate with Cu catalytic sites, and making it possible for further hydrogenation rather than desorption to produce CO or HCOOH.[8-9] Based on the above analysis, both photosensitive units with suitable LUMO energy levels and copper-based active sites are required for a PECR catalyst to have high activity and high selectivity in CO_2 reduction into hydrocarbons. Metal-organic frameworks (MOFs) are constructed by self-assembly of metal ions or metal

clusters with organic linkers.[24-26] Through altering ligands or catalytically active sites can expediently lead to various functional MOFs, making them the promising catalysts for PECR. Some organic materials bearing large π-conjugated structures usually possess narrow band gaps,[27-31] thus making the LUMO energy levels may match well with the reduction potential of CO_2/CH_4. Therefore, a MOF constructed by the copper ions and large π-conjugated ligands may be anticipated to serve as an ideal model for studying and realizing light-induced improvement of the electrocatalytic efficiency for reducing CO_2 to CH_4.

$(H_2NC_2H_6)_6[Cu_2O(dbc)]$ (Cu-DBC, H_8dbc = dibenzo-[*g*,*p*]chrysene-2,3,6,7,10,11,14,15-octaol) possesses a 4-fold interpenetration structure,[32] in which each dbc^{8-} linker coordinates with four copper atoms, each copper ion is coordinated by four oxygen atoms from two catecholate ligands in the same layer and a single oxygen bridge in a distorted square-pyramidal fashion to form a CuO_5 node, and a pair of copper atoms from two adjacent layers are connected by the single oxygen bridges (Figure 1a-b). Such a 3D framework structure based on large π-conjugated organic ligands and square-pyramidal CuO_5 nodes could be a potential PECR catalyst. In this work, Cu-DBC was employed to investigate the structure and performance for selective conversion of CO_2. Interestingly, with the assistance of light, the Faradaic efficiency (FE) of CH_4 and the current density were significantly enhanced over a wide potential range compared to those under the dark environment for Cu-DBC, indicating that the coupling of light energy plays an important role.

Cu-DBC was prepared by hydrothermal method according to the literature.[32] The purity of the as-prepared sample was demonstrated by the scanning electron microscopy (SEM) images and powder X-ray diffraction (PXRD) measurement (Figure S2-3). The electron paramagnetic resonance (EPR) spectrum was consistent with X-ray photoelectron spectroscopy (XPS) (Figure S4), indicating the existence of Cu(II) in the synthesized samples. To study the potential semiconductive property of Cu-DBC, band gap energy (E_g) was determined to be 1.68 eV by Tauc plot (Figure S5). The Mott–Schottky measurements revealed that Cu-DBC was a typical *n*-type semiconductor and its LUMO position located in -0.27 V *vs.* RHE, which is very near to the reduction potential of CO_2/CH_4 (-0.24 V) (Figure 1c). Additionally, we conducted a photocurrent response test to investigate the light absorption capabilities of Cu-DBC, as shown in Figure 1d, revealing that the current density increases obviously under the trigger of light excitation, indicating that effective carrier generation and transfer in Cu-DBC.[33]

In order to investigate the photocatalytic activity of Cu-DBC, we conducted a photocatalytic CO_2RR in a quartz cell with saturated CO_2, triethanolamine (TEOA) as sacrificial electron donor, and without photosensitizer. As shown in Figure S6, the amount of CH_4 was 0.025 μmol (*i.e.* 1.04 μmol g^{-1}•h^{-1}) after 24 hrs and only trace CO was detected, suggesting that Cu-DBC is capable of converting CO_2 into CH_4 with nearly 100% selectivity under visible-light irradiation. However, the reaction rate is poor, which might be ascribed to the limited kinetic process.[34] It is worth mentioning that the applied bias voltage can

promote the separation of photogenerated electrons and holes and enhance the photocatalytic efficiency.[35-36] Therefore, we further evaluated the photoelectrochemical reduction of CO_2 for Cu-DBC.

Results

The photoelectrochemical reduction of CO_2 was tested in 0.1 M $KHCO_3$ aqueous solution. All the potentials mentioned in this work are based on the reversible hydrogen electrode (RHE). The linear sweep voltammetry (LSV) (Figure 2a) revealed that compared with dark condition, the current density of Cu-DBC increases evidently under visible light irradiation (λ > 400 nm). ^{1}H nuclear magnetic resonance (NMR) spectrum (Figure S7) and gas chromatography results (Figures 2b-c) revealed that no liquid-phase products were generated during CO_2 reduction over Cu-DBC. The FEs of different reduced products were tested (Figure 2b), showing the total FEs of gaseous products at all potentials are ~100%. In particular, the FE of CH_4 can reach up to 93.2% with the current density of 10.4 A g^{-1} at -1.4 V, which is the best one among all known MOFs for CH_4 production in CO_2RR (Table S1). Actually, to our best knowledge, only a FN-CTF-400 compound exhibits a higher FE (FE_{CH4} = 99.3%) than Cu-DBC, but with a current density of only 0.2 A g^{-1}.[37] In order to explore the effect of light irradiation, the electrocatalytic CO_2RR was tested in the same potential range without light irradiation (Figure 2c). By comparison, the maximal FE and current density of CH_4 significantly decrease from ~93% to ~54%, and from 10.4 to 3.9 A g^{-1}, respectively, at -1.4 V. This phenomenon indicates that the large *π*-conjugated ligand could serve as a photoswitch to regulate electron transfer pathway to the metal center, and coupling light with electric field can indeed improve the catalytic performance of Cu-DBC for CO_2RR.

In addition to high activity and selectivity, long-term stability is an important factor for PECR catalysts. The *i-t* test was conducted at -1.4 V for 4 hours (Figure 2d), and it showed the current density was changed into 97% of the previous level. Meanwhile, the PXRD patterns, transmission electron microscopy (TEM) images and XPS analysis of Cu-DBC showed negligible change and no generation of Cu_2O or Cu cluster after the CO_2RR test for 4 hours (Figure S8-S9), suggesting that Cu-DBC is stable and the catalytical performance can be ascribed to the MOF rather than Cu_2O or Cu clusters. In the literature,[14] the square-planar CuO_4 nodes of MOF was unstable during the electrocatalytic process, highlighting the high stability of the square-pyramidal CuO_5 nodes in Cu-DBC.

A variety of products can be produced in CO_2 reduction reaction due to the different reaction intermediates formed over the catalysts. In order to investigate the reaction paths occurred on the Cu-DBC, *in-situ* attenuated total reflection infrared (ATR-FTIR) spectral measurements were performed with a home-made cell. Three bands located at 1288, 1366~1383, and 1616 cm^{-1} are associated with the OH-deformation, C–O stretching vibration and O–C=O asymmetric stretching vibration of *COOH intermediate, respectively, while a weaker band at 1020 cm^{-1} belongs to *CHO intermediate (Figures 3a,b).[38-40] Especially, both the *COOH and *CHO groups are crucial intermediates for the reduction of CO_2 to CH_4. Based on the ATR-FTIR spectral analysis, a possible reaction mechanism of the reduction of CO_2

is proposed in Figure 3c. In words, a CO_2 molecule can be physically adsorbed on the square-pyramidal CuO_5 node of Cu-DBC and undergoes a proton-coupled electron transfer process to generate a *COOH intermediate, and then a *CO intermediate, which is successively hydrogenated into *CHO, *OCH_2 and *OCH_3 intermediates, and ultimately achieve the 8-electron transfer process to generate CH_4.

In order to confirm the reaction mechanism, we used periodic density functional theory (PDFT) to simulate the reaction path and evaluate the corresponding energy barriers. As shown in the Figure 3d, the hydrogenation of *CO to *CHO involves a minimum barrier of -0.39 eV, while the production of CO involves a higher barrier of 0.18 eV. The low energy barrier allows the hydrogenation of *CO to be the main reaction. In fact, the energy barriers of hydrogenations of other intermediates are all lower than that of desorption (Figure 3d), which finally results in CH_4 as the main product rather than formic acid, formaldehyde or methanol. The structures of all intermediates obtained by PDFT calculations are illustrated in Figure S10. Comparing with the high energy barrier of hydrogen evolution reaction (Figure S11), the catalytic reduction of CO_2 to CH_4 involves lower energy, which is consistent with the experimental results. These facts suggest that the square-pyramidal CuO_5 nodes of Cu-DBC indeed can serve as the active sites for catalytic reduction of CO_2 to CH_4.

Finally, the significant increase of the FE for CH_4 when coupling light with electrocatalytic CO_2RR can be rationalized to that the formation of methane is thermodynamically feasible, but it must undergo a slow 8-electron transfer process. Through analyzing the frontier orbitals of Cu-DBC, it can be seen that the highest occupied molecular orbital (HOMO) is mainly located on the large π-conjugated ligand, and the lowest unoccupied molecular orbital (LUMO) is mainly located on the metal center. Under dark condition, electrons can enter the LUMO orbital but need a high overpotential to cross the HOMO-LUMO energy gap, resulting in a poor methane yield under dark condition. When Cu-DBC is light irradiated, the electrons in HOMO orbital can harvest photons and jump into the LUMO orbitals that match with the reduction potential of CH_4, then can activate and reduce CO_2 molecule into CH_4 with a high selectivity.

To clarify the mechanism of photo-electrocatalysis and the effect of visible light, the electronic properties of S1 and T1 excited states of Cu-BDC were further calculated with PDFT. Both S1 and T1 exhibit clearly the ligand-to-metal charge-transfer (LMCT) excitation characteristic, which obviously facilitates the electron-flow and CO_2 activation occurring on the square-pyramidal CuO_5 node. When Cu-DBC is light irradiated, the large π-conjugated ligand is first excited from the S_0 ground state to the S_1 state, and then spontaneously transformed to T_1 triplet state through the process of intersystem crossing. The energy gap between S_0 and S_1 is 1.71 eV, which is consistent with the band gap (1.68 eV) calculated from the UV-vis absorption spectrum, confirming the accuracy of the calculations. Since all the photophysical processes occur much faster than the electrocatalysis process, it can be proposed that the photo-coupled electrocatalysis of CO_2 proceeds mainly from the T_1 state rather than the S_0 state. The energy of T_1 is 1.13 eV higher than the S_0 state, suggesting that under light conditions, Cu-DBC will be excited to a higher energy state. Such high energy can enhance the electron transfer from the ligand to the active center,

resulting in the improvement of current density (Figure 2a). These explain the inherent reason why Cu-DBC exhibits high performance for electrocatalytic reduction of CO_2 to CH_4.

Discussion

In summary, a Cu-catecholate based MOF with active CuO_5 sites exhibits excellent activity and selectivity for CH_4 in PECR measurements. Compared with the condition of dark, the FE(CH_4) and current density increase very significantly upon light irradiation. Experimental and theoretical studies reveal that the high performance for PECR is ascribed to the highly catalytical activity of the CuO_5 node, the suitable conduction band edge position and the external light-field can enhance the electron transfer to the adsorbed CO_2. The results provide a new strategy to design and utilize photo-electrocatalysts with light harvesting and catalytic active sites for converting CO_2 into high-valued chemicals.

Methods

Materials and general methods. The ligand dibenzo-[g,p]chrysene-2,3,6,7,10,11,14,15-octaol was synthesized according to the literature.[41] Other reagents were commercially available and without further purification. Power X-ray diffraction (PXRD) patterns were collected on a Bruker D8 Advance diffractometer (Cu Kα). X-ray photoelectron spectroscopy (XPS) measurements were performed on an ESCALAB 250 spectrometer. A SU8010 scanning electron microscope was utilized to investigate the morphology of Cu-DBC. High resolution images of microcrystalline powder of Cu-DBC before and after CO_2 reduction reaction were obtained by a transmission electron microscope (TEM). ^{1}H Nuclear magnetic resonance (^{1}H NMR) measurements were performed on a Bruker advance III. Attenuated total reflection infrared (ATR-FTIR) spectra were recorded on a Nicolet 6700 (Thermo Fisher) to study the reaction intimidates formed over Cu-DBC in the electrochemical measurements.

Synthesis of Cu-DBC. dibenzo-[*g,p*]chrysene-2,3,6,7,10,11,14,15-octaol (8.6 mg) and $Cu(OAc)_2$ (6 mg) were dissolved in 500 μL DMF and 2 mL deionized water. After ultrasonic treatment for 30 minutes, the vessel was placed in an oven with the temperature of 85 °C for 72 hours. Then the MOF was separated from the reaction mixtures by washing with water and dried overnight in 60 °C to obtain the black product.

References

1 Asadi, M. et al. Nanostructured transition metal dichalcogenide electrocatalysts for CO_2 reduction in ionic liquid. *Science* ***353***, 467. (2016)

2 Mikkelsen, M.; Jørgensen, M.; Krebs, F. C. The teraton challenge. A review of fixation and transformation of carbon dioxide. *Energy Environ. Sci.* ***3***, 43-81. (2010)

3 Leung, D. Y. C.; Caramanna, G.; Maroto-Valer, M. M. An overview of current status of carbon dioxide capture and storage technologies. *Renew. Sust. Energ. Rev.* ***39***, 426-443. (2014)

4 Kainiemi, L.; Eloneva, S.; Toikka, A.; Levänen, J.; Järvinen, M. Opportunities and obstacles for CO_2 mineralization: CO_2 mineralization specific frames in the interviews of Finnish carbon capture and storage (CCS) experts. *J. Clean. Prod.* ***94***, 352-358. (2015)

5 Li, C. W.; Ciston, J.; Kanan, M. W. Electroreduction of carbon monoxide to liquid fuel on oxide-derived nanocrystalline copper. *Nature* ***508***, 504-507. (2014)

6 Lin, S. et al. Covalent organic frameworks comprising cobalt porphyrins for catalytic CO_2 reduction in water. *Science* ***349***, 1208. (2015)

7 Jiang, K. et al. Metal ion cycling of Cu foil for selective C–C coupling in electrochemical CO_2 reduction. *Nat. Catal.* ***1***, 111-119. (2018)

8 Nie, X.; Esopi, M. R.; Janik, M. J.; Asthagiri, A. Selectivity of CO_2 reduction on copper electrodes: the role of the kinetics of elementary steps. *Angew. Chem. Int. Ed.* ***52***, 2459-62. (2013)

9 Calle-Vallejo, F.; Koper, M. T. Theoretical considerations on the electroreduction of CO to C_2 species on Cu(100) electrodes. *Angew. Chem. Int. Ed.* ***52***, 7282-5. (2013)

10 Kim, C. et al. Alloy Nanocatalysts for the Electrochemical Oxygen Reduction (ORR) and the Direct Electrochemical Carbon Dioxide Reduction Reaction (CO_2RR). *Adv. Mater.* ***31***, e1805617. (2019)

11 Wesselbaum, S.; vom Stein, T.; Klankermayer, J.; Leitner, W. Hydrogenation of Carbon Dioxide to Methanol by Using a Homogeneous Ruthenium–Phosphine Catalyst. *Angew. Chem. Int. Ed.* ***51***, 7499-7502. (2012)

12 Wang, Y. et al. Hydroxide Ligands Cooperate with Catalytic Centers in Metal–Organic Frameworks for Efficient Photocatalytic CO_2 Reduction. *J. Am. Chem. Soc.* ***140***, 38-41. (2017)

13 Zhong, H. et al. Covalent Organic Framework Hosting Metalloporphyrin-Based Carbon Dots for Visible-Light-Driven Selective CO_2 Reduction. *Adv. Funct. Mater.* ***30***, e2002654. (2020)

14 Nam, D. H. et al. Metal-Organic Frameworks Mediate Cu Coordination for Selective CO_2 Electroreduction. *J. Am. Chem. Soc.* ***140***, 11378-11386. (2018)

15 Zhong, H. et al. Synergistic electroreduction of carbon dioxide to carbon monoxide on bimetallic layered conjugated metal-organic frameworks. *Nat. Commun.* ***11***, 1409. (2020)

16 Schreier, M. et al. Covalent Immobilization of a Molecular Catalyst on Cu_2O Photocathodes for CO_2 Reduction. *J. Am. Chem. Soc.* ***138***, 1938-46. (2016)

17 Lan, Y. Q. et al. Ultrastable Dioxin-Linked Metallophthalocyanine Covalent Organic Frameworks as Photo-Coupled Electrocatalysts for CO_2 Reduction. *Angew. Chem. Int. Ed.* (2020)

18 Chu, S. et al. Photoelectrochemical CO_2 Reduction into Syngas with the Metal/Oxide Interface. *J. Am. Chem. Soc.* ***140***, 7869-7877. (2018)

19 Huang, X.; Shen, Q.; Liu, J.; Yang, N.; Zhao, G. A CO_2 adsorption-enhanced semiconductor/metal-complex hybrid photoelectrocatalytic interface for efficient formate production. *Energy Environ. Sci.* ***9***, 3161-3171. (2016)

20 Jang, J.-W. et al. Aqueous-Solution Route to Zinc Telluride Films for Application to CO_2 Reduction. *Angew. Chem. Int. Ed.* ***53***, 5852-5857. (2014)

21 Chang, X. et al. Stable Aqueous Photoelectrochemical CO_2 Reduction by a Cu_2O Dark Cathode with Improved Selectivity for Carbonaceous Products. *Angew. Chem. Int. Ed.* ***55***, 8840-5. (2016)

22 Yang, D. et al. Visible-light-switched electron transfer over single porphyrin-metal atom center for highly selective electroreduction of carbon dioxide. *Nat. Commun.* ***10***, 3844. (2019)

23 Zhou, B. et al. A GaN:Sn nanoarchitecture integrated on a silicon platform for converting CO_2 to HCOOH by photoelectrocatalysis. *Energy Environ. Sci.* ***12***, 2842-2848. (2019)

24 Furukawa, H.; Cordova, K. E.; O'Keeffe, M.; Yaghi, O. M. The chemistry and applications of metal-organic frameworks. *Science* ***341***, 1230444. (2013)

25 Yang, D.-A.; Cho, H.-Y.; Kim, J.; Yang, S.-T.; Ahn, W.-S. CO_2 capture and conversion using Mg-MOF-74 prepared by a sonochemical method. *Energy Environ. Sci.* ***5***, 6465-6473. (2012)

26 Zhang, J.-P.; Zhang, Y.-B.; Lin, J.-B.; Chen, X.-M. Metal Azolate Frameworks: From Crystal Engineering to Functional Materials. *Chem. Rev.* ***112***, 1001-1033. (2012)

27 Li, Y. et al. Integrating bimetallic AuPd nanocatalysts with a 2D aza-fused π-conjugated microporous polymer for light-driven benzyl alcohol oxidation. *Chinese Chem Lett* ***31***, 231-234. (2020)

28 Mikie, T.; Osaka, I. Small-bandgap quinoid-based π-conjugated polymers. *J. Mater. Chem. C* ***8***, 14262-14288. (2020)

29 Giri, D.; Raut, S. K.; Patra, S. K. Diketopyrrolopyrrole/perylene-diimide and thiophene based D-π-A low bandgap polymer sensitizers for application in dye sensitized solar cells. *Dyes Pigments* ***174***, 108032. (2020)

30 Zheng, L. et al. Solution-processed broadband polymer photodetectors with a spectral response of up to 2.5 μm by a low bandgap donor–acceptor conjugated copolymer. *J. Mater. Chem. C* ***6***, 3634-3641. (2018)

31 Weldeab, A. O. et al. Pyridine-terminated low gap π-conjugated oligomers: design, synthesis, and photophysical response to protonation and metalation. *Org. Chem. Front.* ***5***, 3170-3177. (2018)

32 Liu, J. et al. Conjugated Copper-Catecholate Framework Electrodes for Efficient Energy Storage. *Angew. Chem. Int. Ed.* ***59***, 1081-1086. (2020)

33 Pan, A. et al. $CsPbBr_3$ Perovskite Nanocrystal Grown on MXene Nanosheets for Enhanced Photoelectric Detection and Photocatalytic CO_2 Reduction. *J. Phys. Chem. Lett.* ***10***, 6590-6597. (2019)

34 Chang, K.; Zhang, H.; Chen, J. G.; Lu, Q.; Cheng, M.-J. Constant Electrode Potential Quantum Mechanical Study of CO_2 Electrochemical Reduction Catalyzed by N-Doped Graphene. *ACS Catal.* ***9***, 8197-8207. (2019)

35 Cortes, M. A. L. R. M. et al. Photoelectrochemical reduction of CO_2 with TiNT. *Mat Sci in Semicon Proc* ***108***, (2020)

36 Xie, S.; Zhang, Q.; Liu, G.; Wang, Y. Photocatalytic and photoelectrocatalytic reduction of CO_2 using heterogeneous catalysts with controlled nanostructures. *Chem. Commun.* ***52***, 35-59. (2016)

37 Wang, Y.; Chen, J.; Wang, G.; Li, Y.; Wen, Z. Perfluorinated Covalent Triazine Framework Derived Hybrids for the Highly Selective Electroconversion of Carbon Dioxide into Methane. *Angew. Chem. Int. Ed.* ***57***, 13120-13124. (2018)

38 Yi, J. D. et al. Highly Selective CO_2 Electroreduction to CH_4 by In Situ Generated Cu_2O Single-Type Sites on a Conductive MOF: Stabilizing Key Intermediates with Hydrogen Bonding. *Angew. Chem. Int. Ed.* ***59***, 23641-23648. (2020)

39 Li, X. et al. Selective visible-light-driven photocatalytic CO_2 reduction to CH_4 mediated by atomically thin $CuIn_5S_8$ layers. *Nat. Energy* ***4***, 690-699. (2019)

40 Wang, T. et al. Photoreduction of CO_2 over the well-crystallized ordered mesoporous TiO_2 with the confined space effect. *Nano Energy* ***9***, 50-60. (2014)

41 Varshney, S. K.; Nagayama, H.; Takezoe, H.; Prasad, V. Octasubstituted dibenzochrysenes: discotic liquid crystals with a twisted core. *Liq. Cryst.* ***36***, 1409-1415. (2009)

Declarations

Acknowledgements

This work was supported by the NSFC (21890380, 21821003), Local Innovative and Research Teams Project of Guangdong Pearl River Talents Program (2017BT01C161), and Guangdong Natural Science Funds for Distinguished Young Scholar (2018B030306009).

Author contributions

P.Q.L. designed the research. Y.Y.L., H.L.Z. and N.Y.H. performed syntheses and measurements. Y.Y.L., P.Q.L. and X.M.C. wrote the manuscript.

Competing financial interests

The authors declare no competing financial interests.

Scheme

Scheme 1 is available in the Supplementary Files.

Figures

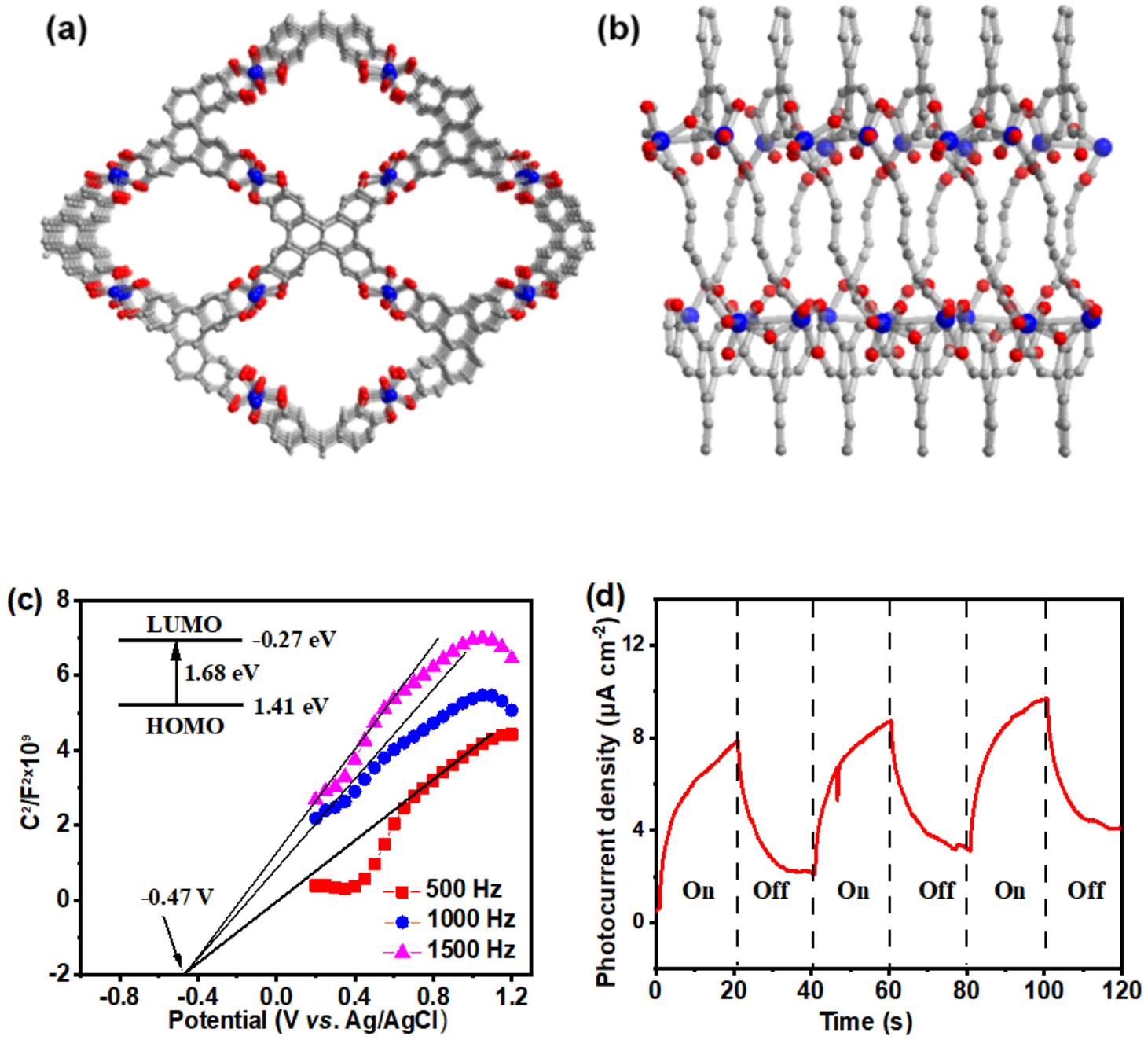

Figure 1

Structure analysis and Photocurrent response measurement. (a) Top and (b) side views of Cu-DBC. Color codes: Cu, blue; O, red; C, grey. (c) Mott-Schottky plots of Cu-DBC. (d) Photocurrent response at -1.0 V vs. Ag/AgCl on Cu-DBC.

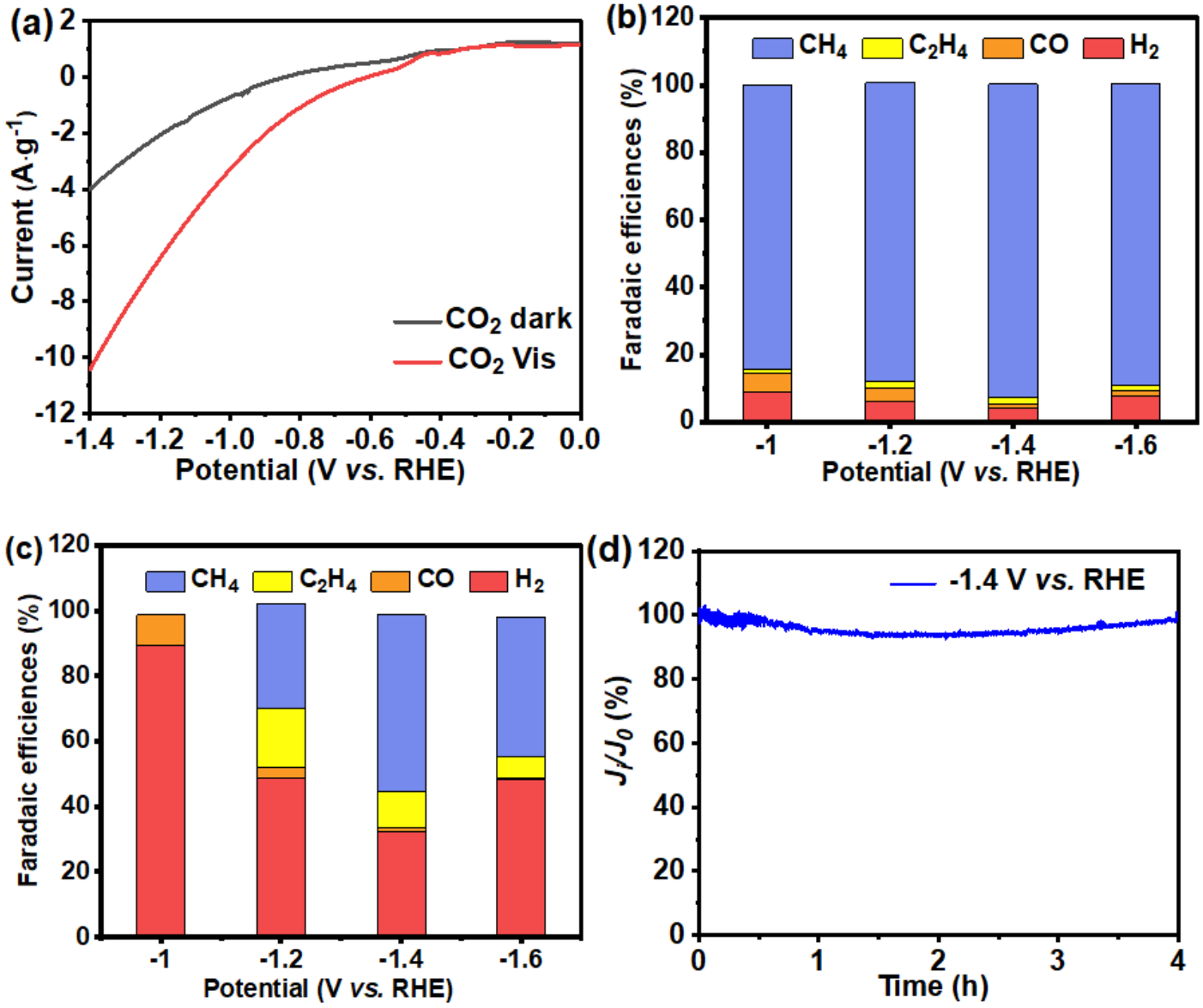

Figure 2

Evaluation of catalytic performance. (a) LSV curves of Cu-DBC scanned at 0.1 V s-1 in CO2-saturated 0.1 M KHCO3 under visible light and dark conditions at -1.4 V for 4 h. (b) The FEs of different reduced products were tested at the potentials of -1.0 to -1.6 V under visible light and (c) under dark condition. (d) Durability test plot of Cu-DBC.

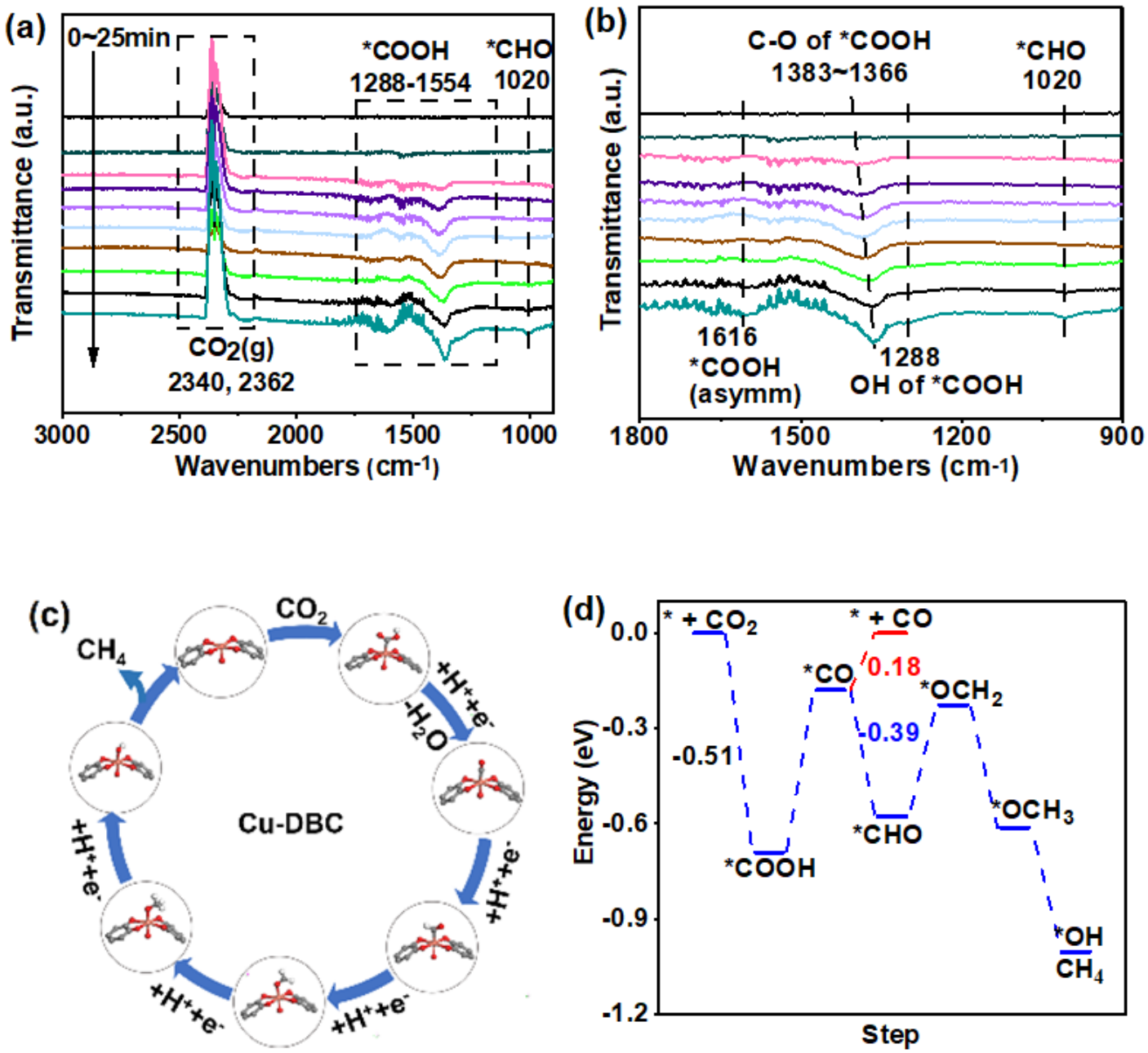

Figure 3

Mechanism analysis. (a-b) Operando ATR-FTIR spectra of Cu-DBC collected in CO2 saturated 0.1 M KHCO3 electrolyte. (c) Proposed reaction path for photo-coupled CO2 electroreduction for the square-pyramidal CuO5 node of Cu-DBC. (d) Illustration of the energy barriers of CO2 reduction to CH4 or CO over Cu-DBC.

Supplementary Files

This is a list of supplementary files associated with this preprint. Click to download.

- Scheme1.png
- SI.pdf